Full-dimensional quantum dynamics of rovibrationally inelastic scattering between CN and H2

Benhui Yang, X. H. Wang, P. C. Stancil, J. M. Bowman, N. Balakrishnan, and R. C. Forrey

Citation: J. Chem. Phys. **145**, 224307 (2016); doi: 10.1063/1.4971322
View online: http://dx.doi.org/10.1063/1.4971322
View Table of Contents: http://aip.scitation.org/toc/jcp/145/22
Published by the American Institute of Physics

RIGHTSLINK

Full-dimensional quantum dynamics of rovibrationally inelastic scattering between CN and H_2

Benhui Yang,[1] X. H. Wang,[2] P. C. Stancil,[1] J. M. Bowman,[2] N. Balakrishnan,[3] and R. C. Forrey[4]

[1]*Department of Physics and Astronomy and the Center for Simulational Physics, The University of Georgia, Athens, Georgia 30602, USA*
[2]*Department of Chemistry, Emory University, Atlanta, Georgia 30322, USA*
[3]*Department of Chemistry, University of Nevada, Las Vegas, Nevada 89154, USA*
[4]*Department of Physics, Penn State University, Berks Campus, Reading, Pennsylvania 19610, USA*

(Received 6 September 2016; accepted 20 November 2016; published online 13 December 2016)

We report six-dimensional (6D) potential energy surface (PES) and rovibrational scattering calculations for the CN–H_2 collision system. The PES was computed using the high-level *ab initio* spin-restricted coupled-cluster with single, double, and perturbative triple excitations-F12B method and fitted to an analytic function using an invariant polynomial method in 6D. Quantum close-coupling calculations are reported for rotational transitions in CN by H_2 and D_2 collisions in 6D as well as four-dimensional (4D) within a rigid rotor model for collision energies of 1.0-1500 cm^{-1}. Comparisons with experimental data and previous 4D calculations are presented for CN rotational levels j_1 = 4 and 11. For the first time, rovibrational quenching cross sections and rate coefficients of CN (v_1 = 1, j_1 = 0) in collisions with *para*- and *ortho*-H_2 are also reported in full-dimension. Agreement for pure rotational transitions is found to be good, but no experimental data on rovibrational collisional quenching for CN–H_2 are available. Applications of the current rotational and rovibrational rate coefficients in astrophysical modeling are briefly discussed. *Published by AIP Publishing.* [http://dx.doi.org/10.1063/1.4971322]

I. INTRODUCTION

The hydrogen molecule is the dominant species in the vast majority of interstellar environments, while the cyano radical (CN) is also relatively abundant. Both may play important roles in the physics and chemistry of diffuse clouds, for example. CN is mainly observed via visible absorption in diffuse and translucent clouds,[1,2] and it is also detected in the millimeter where it can be important in the chemistry of dense molecular clouds. Ever since it was identified by McKellar in 1940,[3] CN has been detected in a variety of molecular clouds.[4–8] For example, Wootten *et al.*[4] reported the first observations of the $N = 2-1$ line at 226.9 GHz in the circumstellar envelope of the carbon-rich star IRC + 10216 and in the Orion Molecular Cloud (OMC-1). CN is also believed to be an excellent tracer of photodissociation regions (PDRs) which are environments exposed to intense ultraviolet (UV) radiation.[9,10] To model the infrared radiation from CN in such environments requires a rich variety of molecular data, including inelastic rotational and vibrational collision rate coefficients, primarily due to H_2. However, because of the difficulty of measurements of these quantities, numerical models often rely on theoretical rates. While state-to-state inelastic rotational (de)excitation rate coefficients due to H_2 collisions were measured for the vibrationally excited state $v_1 = 2$ by Brunet *et al.*,[11] no data are available for vibrationally inelastic transitions in CN induced by H_2.

Due to its fundamental and astrophysical importance, the CN–H_2 collisional system has been the subject of many theoretical[12–18] and experimental[11,19] studies. An early four-dimensional (4D) potential energy surface (PES) within the rigid-rotor model was obtained by Kaledin *et al.*[12] and applied to a study of the spectroscopy of the CN–H_2 van der Waals complex. More recently, Kalugina *et al.*[14,15] calculated a 4D PES using the partially spin-restricted coupled-cluster with single, double, and perturbative triple excitations (RCCSD(T)) method and an aug-cc-pVTZ basis set augmented by 3*s*, 2*p*, 1*d* bond functions. Fine- and hyperfine-resolved collisional excitation calculations of CN ($v_1 = 0$) with *para*-H_2 ($v_2 = 0$, $j_2 = 0$) were performed, but using a two-dimensional (2D) PES obtained by averaging the 4D PES over the H_2 angular degrees of freedom. Later, the 4D PES of Kalugina *et al.*[14,15] was used in close-coupling (CC) calculations of rotational de-excitation cross section of CN ($v_1 = 0$) by *para*- and *ortho*-H_2.[15] In both PES and scattering calculations,[14,15] fixed bond distances (i.e., equilibrium bond distance of CN at $r_1 = 2.2144$ a_0 and vibrationally averaged bond distance of H_2 at $r_2 = 1.4487$ a_0) were adopted. Recently, the 4D PES of Kalugina and Lique was also applied to calculate fine- and hyperfine-resolved rotational excitation rate coefficients of CN with *para*- and *ortho*-H_2[17] and of CN isotopologues, ^{13}CN and $C^{15}N$, by *para*-H_2.[18]

To go beyond the rigid-rotor approximation, in this work we have constructed a full dimensional (6D) PES for the CN–H_2 system and carried out comprehensive CC calculations of state-to-state cross sections in an effort to initiate the development of a complete database of rovibrational quenching rate coefficients. In Secs. II–V, the 6D PES calculations, the adopted scattering approach, and the results are

RIGHTSLINK

discussed. Conclusions are presented in Sec. VI. Transitions at the fine- or hyperfine-resolved level are not considered here.

II. THE POTENTIAL ENERGY SURFACE

The electronic ground state interaction potential of CN–H_2 was computed using the explicitly correlated coupled-cluster (RCCSD(T)-F12B) method,[20,21] with an aug-cc-pVTZ basis,[22] as implemented in MOLPRO 2010.1.[23] The interaction energies were calculated using the supermolecular approach in which the counter-poise (CP)[24] correction was employed to reduce the basis set superposition error (BSSE).[25] To construct the PES, the computations were performed on a 6D grid using Jacobi coordinates as shown in Fig. 1. The radial coordinate R denotes the distance between the center-of-masses of CN and H_2, while r_1 and r_2 represent the bond lengths of CN and H_2, respectively. The angular coordinates θ_1 and θ_2 denote, respectively, the angle between $\vec{r}_1$ and $\vec{R}$ and $\vec{r}_2$ and $\vec{R}$, while ϕ denotes the out-of-plane dihedral angle. For the potential energy calculations, the bond lengths of H_2 and CN spanned the range 1.1011–1.8011 a_0 and 2.0184–2.5184 a_0, respectively. R is scanned from 5 to 21 a_0 with a step-size of 0.5 a_0 for $R < 8$ a_0 and 1.0 a_0 for $R > 8$ a_0. The angle θ_1 ranges from 0° to 180° with a step-size of 22.5°, and θ_2 and ϕ have range 0° to 180° and 0° to 90°, respectively, with a step-size of 30°. The range of r_1 and r_2 allows for the treatment of vibrational excitation up to $v_1 = 2$ for CN, but only for $v_2 = 0$ for H_2, and as the bond lengths do not approach dissociation, rearrangement channels (e.g., to form HCN) are excluded from consideration on this PES. While the barrier to reaction is around 1260 cm^{-1} (3.6 kcal/mol), which is comparable to the CN ($v_1 = 1$) excitation energy, CN plays the role of a spectator in the reaction dynamics because the effective barrier at the saddle point increases by the same energy as the CN ($v_1 = 1$) excitation energy. As a consequence, reaction channels are not incorporated into the PES or scattering.

An invariant polynomial method[26,27] has been used to fit the 6D CN–H_2 interaction PES, which is expanded in the form

$$V(y_1 \cdots y_6) = \sum_{n_1 \cdots n_6}^{N} c_{n_1 \cdots n_6} y_1^{n_1} y_6^{n_6} \left[y_2^{n_2} y_3^{n_3} y_4^{n_4} y_5^{n_5} + y_2^{n_5} y_3^{n_4} y_4^{n_3} y_5^{n_2} \right], \tag{1}$$

where $y_i = e^{-0.5 d_i}$ is a Morse-type variable, d_i are the internuclear distances (in atomic units) between two atoms, $d_1 = d_{HH'}$, $d_2 = d_{NH'}$, $d_3 = d_{CH'}$, $d_4 = d_{CH}$, $d_5 = d_{NH}$, and $d_6 = d_{CN}$. The total power of the polynomial, $N = \sum_{i=1}^{7} n_i$, was restricted to 7.

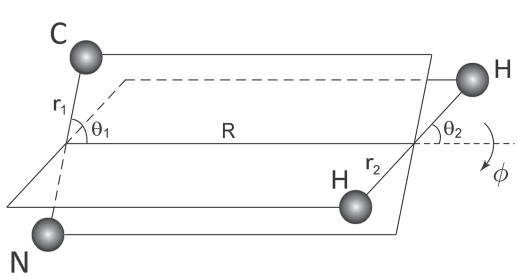

FIG. 1. The six-dimensional Jacobi coordinates for CN–H_2.

TABLE I. Global and local minima on the 4D PESs. V in cm^{-1}, R in bohr.

	V6ES-4D	Reference 15	Reference 12
Global	V = −122.51	V = −121.36	−100.84
	R = 7.21	R = 7.23	7.44
Local	V = −81.98	V = −83.86	−68.44
	R = 7.41	R = 7.39	7.52

The fit for the expansion coefficients $c_{n_1 \ldots n_6}$ was performed using a weighted least-squares method for interaction energies up to 3000 cm^{-1}. The root-mean-square (RMS) error in the PES fit was 3.67 cm^{-1}, which included 84 734 *ab initio* points. The 6D interaction PES, $V(R, r_1, r_2, \theta_1, \theta_2, \phi)$, hereafter referred to as V6ES, can be averaged over the ground-state or excited vibrational wave functions of CN and H_2 to obtain 4D vibrationally averaged PESs, $V(R, \theta_1, \theta_2, \phi)$. However, V6ES was used in the majority of the scattering calculations. The comparison of the global and local minima on the vibrationally averaged V6ES-4D PES and the 4D PESs of Kalugina *et al.*[15] and Kaledin *et al.*[12] is given in Table I. Note that this is not an exact comparison as the 4D PESs were constructed differently.

Some features of the fitted V6ES PES are illustrated in Figs. 2–4. Fig. 2 displays the R dependence of V6ES for various angles and bond distances fixed at $r_1 = r_e(CN) = 2.2144$ a_0 and $r_2 = r_e(H_2) = 1.4011$ a_0. The computed *ab initio* potential energy points are also displayed as symbols. Fig. 3 shows two-dimensional contour plots in θ_1 and θ_2 for the V6ES PES. The CN and H_2 bond lengths are fixed at their equilibrium distances for $R = 3.0$, 3.5, 4.0, and 6.0 Å, $\phi = 0°$, 45°, and 90°. This figure can be compared to Fig. 3 of Kalugina *et al.*[15] and Fig. 2 of Kaledin *et al.*[14] The current Fig. 4 depicts the anisotropy of the V6ES potential in θ_1 for various ϕ. Here θ_1 describes the orientation of CN; the anisotropy with respect to θ_1 is large.

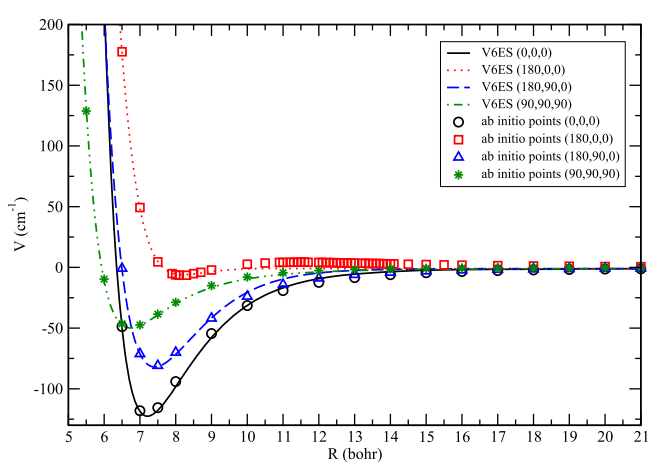

FIG. 2. R dependence of the interaction potential V6ES for representative slices with bond lengths fixed as indicated in the text and (θ_1, θ_2, ϕ) = (0°, 0°, 0°), (180°, 0°, 0°), (180°, 90°, 0°), and (90°, 90°, 90°). V6ES fit (lines), computed *ab initio* energy points (symbols).

RIGHTSLINK

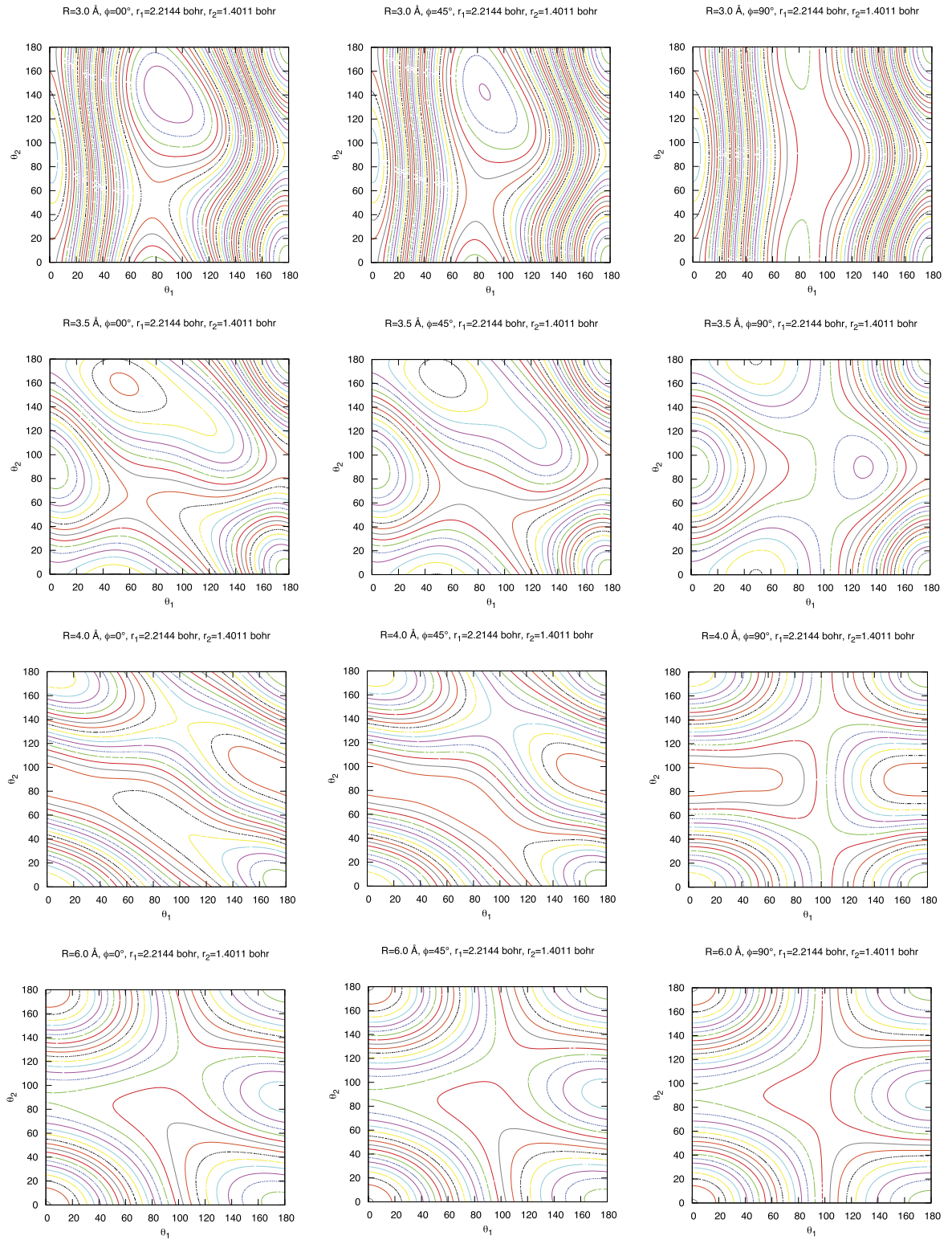

FIG. 3. Contour plots of θ_1 and θ_2. CN and H_2 bond distances r_1 = 2.2144 and r_2 = 1.4011 a_0. The rows correspond to R = 3.0, 3.5, 4.0, and 6.0 Å, while the columns correspond to $\phi = 0°$, 45°, and 90°.

III. SCATTERING METHODS

In the quantum-mechanical description of inelastic molecular scattering, the theory for the collision of two $^1\Sigma$ diatomic molecules within the rigid rotor and vibrating rotor models was developed[28–31] based on the close-coupling (CC) formulation of Arthurs and Dalgarno.[32] Recently the theory has been implemented for the full-dimensional study of the vibrationally inelastic scattering between two diatomic molecules.[33–35] Here, we apply this formalism for the CN + H_2 system by approximating CN as a $^1\Sigma$ molecule,

RIGHTSLINK

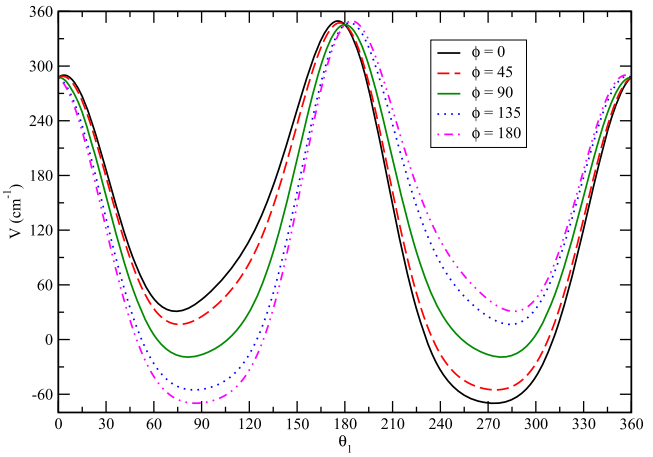

FIG. 4. Comparison of the θ_1 dependence of the V6ES surface for $\phi = 0°$, 45°, 90°, 135°, and 180°. R = 6.0 a_0, $\theta_2 = 45°$, r_1 = 2.2144 a_0, and r_2 = 1.4011 a_0.

hence the rotational quantum number $N_1 = j_1$ since we neglect spin. In the scattering calculations, the interaction PES $V(R, r_1, r_2, \theta_1, \theta_2, \phi)$ was expanded in the form

$$V(R, r_1, r_2, \theta_1, \theta_2, \phi) = \sum_{\lambda_1\lambda_2\lambda_{12}} A_{\lambda_1,\lambda_2,\lambda_{12}}(r_1, r_2, R) \times Y_{\lambda_1,\lambda_2,\lambda_{12}}(\hat{r}_1, \hat{r}_2, \hat{R}), \quad (2)$$

where $Y_{\lambda_1,\lambda_2,\lambda_{12}}$ is a bi-spherical harmonic function given by

$$Y_{\lambda_1,\lambda_2,\lambda_{12}}(\hat{r}_1, \hat{r}_2, \hat{R}) = \sum_{m_{\lambda_1} m_{\lambda_2} m_{\lambda_{12}}} \langle \lambda_1 m_{\lambda_1} \lambda_2 m_{\lambda_2} | \lambda_{12} m_{\lambda_{12}} \rangle \times Y_{\lambda_1 m_{\lambda_1}}(\hat{r}_1) Y_{\lambda_2 m_{\lambda_2}}(\hat{r}_2) Y^*_{\lambda_{12} m_{\lambda_{12}}}(\hat{R}), \quad (3)$$

where $0 \le \lambda_1 \le 8$, $0 \le \lambda_2 \le 4$, and only even values of λ_2 are retained due to the symmetry of H_2.

We use the term combined molecular state (CMS) to describe a combination of rovibrational states of the CN–H_2 scattering system. A CMS, denoted as $(v_1 j_1 v_2 j_2)$, represents a unique quantum state before or after a collision: $v = v_1 v_2$ and $j = j_1 j_2$ denote the vibrational and rotational quantum numbers of the two molecules.

The rovibrational state-to-state cross section as a function of collision energy E is given by

$$\sigma_{v_1 j_1 v_2 j_2 \to v_1' j_1' v_2' j_2'}(E) = \frac{\pi}{(2j_1 + 1)(2j_2 + 1)k^2} \times \sum_{j_{12} j_{12}' l l' J \varepsilon_I} (2J + 1) |\delta_{v_1 j_1 v_2 j_2 l, v_1' j_1' v_2' j_2' l'} - S^{J\varepsilon_I}_{v_1 j_1 v_2 j_2 l, v_1' j'_1 v_2' j_2' l'}(E)|^2, \quad (4)$$

where $(v_1 j_1 v_2 j_2)$ and $(v_1' j_1' v_2' j_2')$ denote the initial and final CMSs, respectively, and l is the orbital angular momentum quantum number. The total angular momentum of the collision system is given by $\vec{J} = \vec{l} + \vec{j}_{12}$ with $\vec{j}_{12} = \vec{j}_1 + \vec{j}_2$ and $k = \sqrt{2\mu E/\hbar^2}$ is the wave vector with respect to the initial channel.

For a given H_2 transition, $j_2 \to j_2'$, the total vibrational quenching cross section of CN from $v_1 \to v_1'$ can be obtained by summing over the final rotational levels j_1' of CN in vibrational state v_1',

$$\sigma^{\mathrm{T}}_{v_1 j_1 v_2 j_2 \to v_1' v_2' j_2'}(E) = \sum_{j_1'} \sigma_{v_1 j_1 v_2 j_2 \to v_1' j_1' v_2' j_2'}(E). \quad (5)$$

In this work, H_2 is taken to remain in its ground vibrational state, $v_2 = v_2' = 0$. However, the CN total vibrational quenching cross sections were calculated for both elastic ($j_2' = j_2$) and inelastic ($j_2' \neq j_2$) H_2 transitions.

All CC scattering calculations were carried out using the TwoBC code[36] with the coupled-channel equations propagated using the log-derivative method of Johnson[37] and Manolopoulos[38] with a radial step-size of ΔR = 0.05 a_0 and the range of R propagation from 5 to 21 a_0. The number of discrete variable representation points N_{r1} and N_{r2}; the number of points in θ_1 and θ_2 for Gauss-Legendre quadrature, N_{θ_1} and N_{θ_2}; and the number of points in ϕ for Chebyshev quadrature, N_ϕ, used to project out the potential expansion coefficients are presented in Table II. The basis sets used in the pure rotational and rovibrational scattering calculations are also presented in Table II.

The state-to-state rate coefficients at a temperature T can be obtained by thermally averaging the corresponding integral cross sections over a Maxwellian kinetic energy distribution,

$$k_{v_1 j_1 v_2 j_2 \to v_1' j_1' v_2' j_2'}(T) = \left(\frac{8}{\pi\mu\beta}\right)^{1/2} \beta^2 \int_0^\infty E\sigma_{v_1 j_1 v_2 j_2 \to v_1' j_1' v_2' j_2'}(E) \times \exp(-\beta E) dE, \quad (6)$$

TABLE II. Parameters used in the TwoBC scattering calculations.

	Basis set[a]	N_{θ_1}	N_{θ_2}	N_ϕ	N_{r1}	N_{r2}	λ_1	λ_2
6D rotational calculation								
para-H_2–CN	$j_1 = 20, j_2 = 2$	12	12	8	18	18	8	4
ortho-H_2–CN	$j_1 = 20, j_2 = 3$	12	12	8	18	18	8	4
6D rovibrational calculation								
para-H_2–CN	[(0,22; 1,20) (0,2)]	12	12	8	18	18	8	4
para-H_2–CN	[(0,22; 1,20) (0,3)]	12	12	8	18	18	8	4

[a]Basis set $[(v_1 = 0, j_{v1=0};\ v_1 = 1, j_{v_1=1})\ (v_2 = 0, j_{v_2=0})]$ is presented by the maximum rotational quantum number j_{v_1} and j_{v_2} included in each relevant vibrational level v_1 and v_2 for CN and H_2, respectively.

RIGHTSLINK

where μ is the reduced mass of the CN–H_2 complex, $\beta = (k_B T)^{-1}$, and k_B is Boltzmann's constant.

IV. RESULTS

A. Pure rotational scattering

We first consider the rotational transitions of CN in collisions with H_2 and D_2 when the molecules remain in their ground vibrational states $v_1 = v_2 = v_1' = v_2' = 0$,

$$\mathrm{CN}(v_1 = 0, j_1) + \mathrm{H_2}(v_2 = 0, j_2) \rightarrow \mathrm{CN}(v_1' = 0, j_1') + \mathrm{H_2}(v_2' = 0, j_2'),$$

and

$$\mathrm{CN}(v_1 = 0, j_1) + \mathrm{D_2}(v_2 = 0, j_2) \rightarrow \mathrm{CN}(v_1' = 0, j_1') + \mathrm{D_2}(v_2' = 0, j_2').$$

Full-dimensional calculations using TwoBC with V6ES and rigid rotor approximation calculations using MOLSCAT[39] with vibrationally averaged 4D PESs have been performed to obtain the rotational excitation and de-excitation cross sections of CN in collisions with H_2. For CN with D_2, only rigid-rotor approximation calculations using vibrationally averaged 4D PESs are carried out. Three vibrationally averaged 4D PESs in the CN ground and excited vibrational states $v_1 = 0$, 1, and 2, referred to as V4H2-0, V4H2-1, and V4H2-2, are computed for CN–H_2. For CN–D_2, the vibrationally averaged 4D PESs are referred to as V4D2-0, V4D2-1, and V4D2-2. In constructing these 4D PESs, H_2 and D_2 are in their ground vibrational state $v_2 = 0$.

The initial rotational state of CN was taken to be $j_1 = 4$ and 11 to make comparisons with available measurements as described below. For *para*-H_2 and *ortho*-D_2, rotational levels $j_2 = 0$ and 2 were included in the basis set while for *ortho*-H_2 and *para*-D_2, $j_2 = 1$ and 3 were included.

Rotational excitation and de-excitation cross sections of CN ($v_1 = 0, j_1 = 4$) in collisions with *para*-H_2 ($v_2 = 0, j_2 = 0$, 2) and *ortho*-H_2 ($v_2 = 0, j_2 = 1$) have been computed for collision energies ranging from 1.0 to 1500 cm^{-1}. In Figs. 5–7, the calculated de-excitation cross sections using V6ES and V4H2-0 are compared with the 4D results of Kalugina *et al.*[15] It can be seen that the 6D V6ES and 4D V4H2-0 PESs yield nearly identical results. The cross sections for de-excitation from $j_1 = 4$ are seen to be in good agreement with the results of Kalugina *et al.*

Brunet *et al.*[11] measured the rotational inelastic, but vibrationally elastic, state-to-state rate coefficients of CN ($X\,^2\Sigma^+, v_1 = 2$) due to collisions with normal H_2 and D_2. For comparison, the state-to-state rotational excitation and de-excitation rate coefficients of CN ($v_1 = 0, j_1 = 4$ and 11) in collisions with H_2 and D_2 with $v_2 = 0, j_2 = 0, 1, 2$ are computed using Eq. (6). The Boltzmann average, over the H_2 and D_2 rotational levels, of the state-to-state rate coefficients $k(j_1 j_2)$ was then obtained with the partition function Q of the first three rotational states of H_2 and D_2 ($j_2 = 0$, 1, 2) and given by

$$\bar{k}(j_1) = \frac{\sum_{j_2=0}^{2} w_{j_2}(2j_2+1)e^{-\epsilon_{j_2}/kT} k(j_1 j_2)}{Q}, \tag{7}$$

where

$$Q = \sum_{j_2=0}^{2} w_{j_2}(2j_2+1)e^{-\epsilon_{j_2}/kT}, \tag{8}$$

$k(j_1 j_2)$ is the rate coefficients from initial CMS ($0j_1 0j_2$), $\epsilon_{j_2} = B_0 j_2(j_2+1)$, the rotational constant B_0 is 59.3219 cm^{-1} for H_2 and 29.9043 cm^{-1} for D_2, and w_{j2} is the spin degeneracy, $w_{j2} = 3$ for *ortho*-H_2 and *para*-D_2 and 1 for *para*-H_2 and *ortho*-D_2.

In Figs. 8 and 9 we compare the present rate coefficients with measurements[11] and the theoretical results of Kalugina *et al.*[15] For collisions with normal H_2 and $j_1 = 4$, the results of full-dimensional calculations using V6ES and rigid-rotor approximation calculations using vibrationally averaged PESs V4H2-0, V4H2-1, and V4H2-2 are displayed in Fig. 8(a). The 4D PESs yield very similar scattering results, which are also comparable to the 6D results. Due to the degeneracy

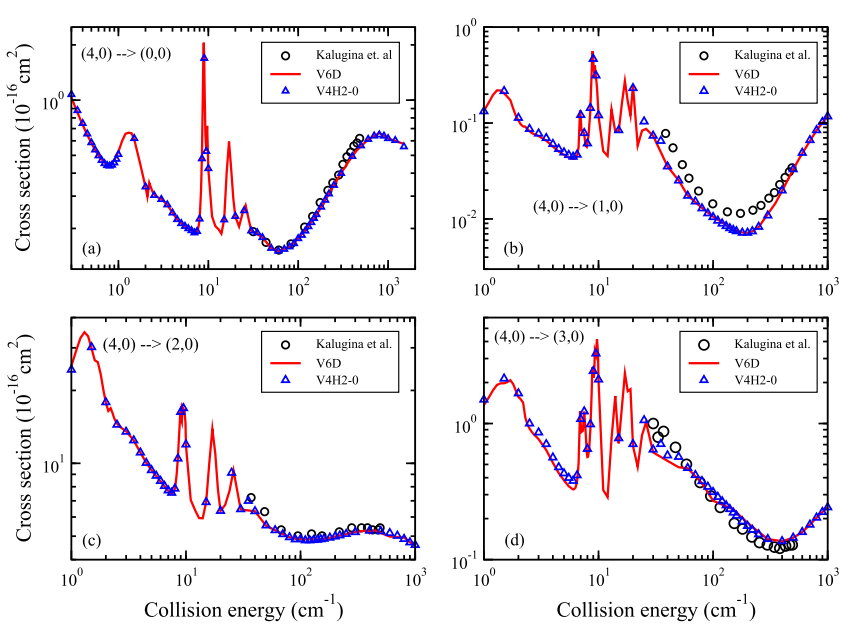

FIG. 5. Rotational de-excitation cross sections for CN ($v_1 = 0, j_1 = 4$) + H_2 ($v_2 = 0, j_2 = 0$) → CN ($v_1' = 0, j_1'$) + H_2 ($v_2' = 0, j_2' = 0$), $j_1' = 0$, 1, 2, and 3 with initial CMS (0400). Current 6D (lines) and 4D-0 (triangles) results and 4D calculations of Ref. 15 (circles).

RIGHTSLINK

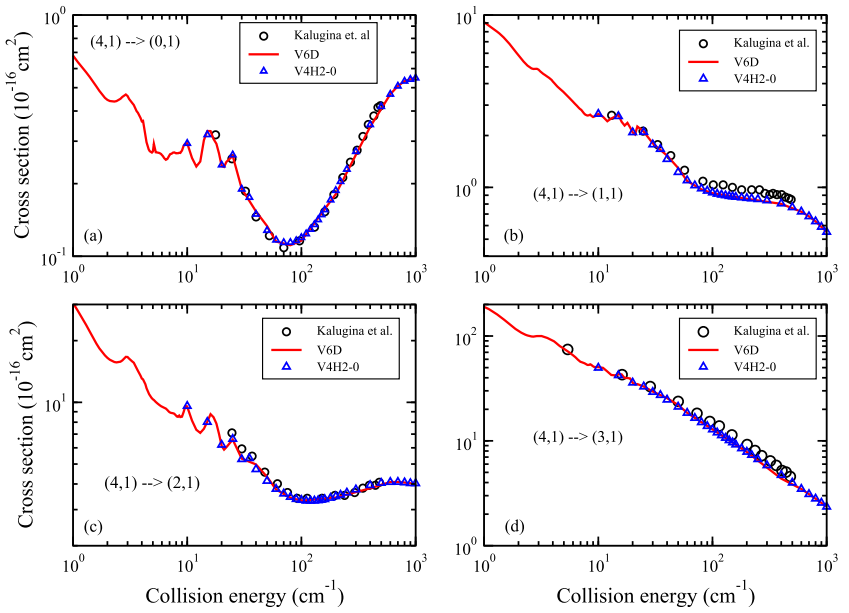

FIG. 6. Same as Figure 5 except for $j_2 = j_2' = 1$, i.e., initial CMS (0401).

factors and assumed relative rotational populations given by Equation (7), the rate coefficients for normal-H_2 are dominated by *ortho*-H_2 transitions. Therefore, while Fig. 5 displays an even Δj_1 propensity rule for *para*-H_2, applicable for a near-homonuclear molecule like CN, an exponential energy-gap-law behavior is evident for *ortho*-H_2 cross sections in Fig. 6. As a consequence, any evidence of an even Δj propensity is washed-out in Fig. 8 with the result that $\Delta j_1 = \pm 1$ dominates. For $j_1 = 11$, presented in Fig. 8(b), the even Δj_1 propensity is partially recovered, though $\Delta j_1 = \pm 1$ transitions give the largest rate coefficients.

For both $j_1 = 4$ and 11, the comparison of the present rate coefficients with experiment and the theoretical results of Kalugina *et al.*[15] shows good agreement particularly in light of the fact that this is an absolute value comparison. The exception occurs for $\Delta j_1 = \pm 1$ transitions where noticeable differences are found between the experiment and all calculations. The calculations of Kalugina *et al.*[15] are somewhat closer to the measurements which are mostly due to their slightly larger (0401) to (0301) cross section (see bottom right panel of Fig. 6).

Fig. 9 shows similar comparisons between our theoretical results of CN in collision with D_2 and measurements.[11] The results from three vibrationally averaged 4D PESs, V4D2-0, V4D2-1, and V4D2-2 are very similar for both $j_1 = 4$ and 11, except that V4D2-2 gives smaller rate coefficients for $\Delta j_1 = \pm 1$ transitions.

While the measurement was performed for vibrationally excited CN ($v_1 = 2$), calculations which used $v_1 = 0$, though for vibrationally averaged PESs, are not direct comparisons. We explored whether this was an issue by repeating our 4D

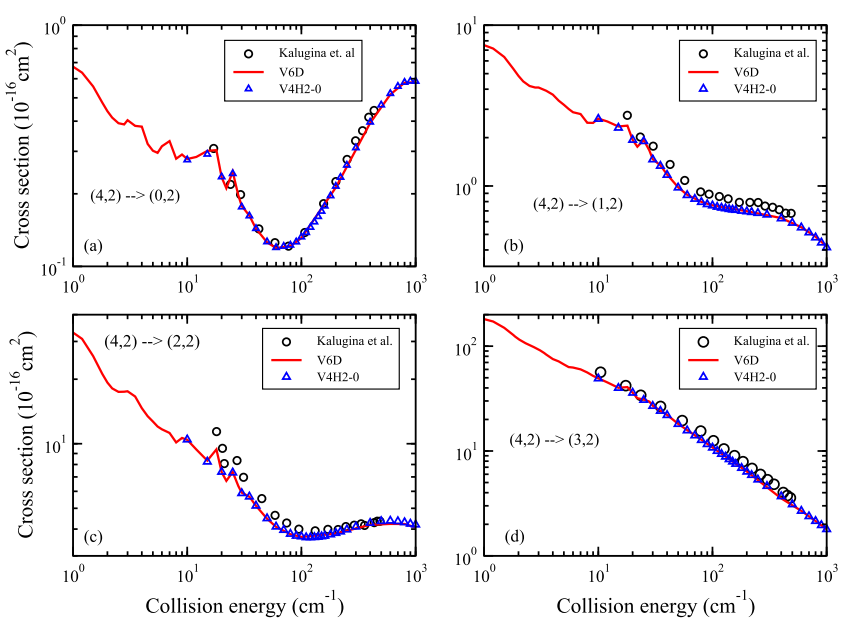

FIG. 7. Same as Figure 5 except for $j_2 = j_2' = 2$, i.e., initial CMS (0402).

RIGHTSLINK

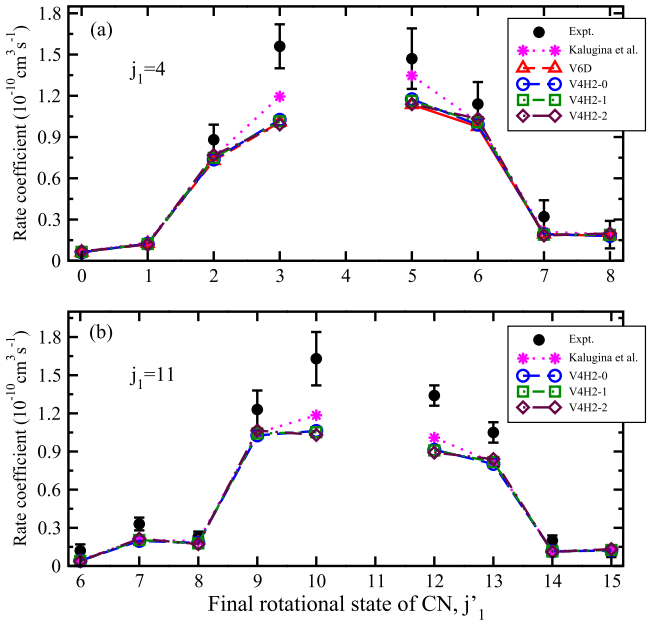

FIG. 8. Inelastic rotational rate coefficients for CN at T = 295 K for a statistical population of H_2 ($v_2 = 0, j_2 = 0, 1$), i.e., normal-H_2. (a) $j_1 = 4$, (b) $j_1 = 11$. Experiment[11] $v_1 = 2$ (solid circles), 4D theory[15] $v_1 = 0$ (stars), and current 6D and 4D theory $v_1 = 0$ (open triangles and open circles), $v_1 = 1$ (open squares), and $v_1 = 2$ (open diamonds).

calculations on $v_1 = 1$ and 2 vibrationally averaged PESs. Figs. 8 and 9 demonstrate that rotational transitions are nearly independent of v_1, except as noted above, the $\Delta j_1 = \pm 1$ transitions are somewhat smaller for D_2 collisions on the V4D2-2, i.e., $v_1 = 2$ surface. This might be related to the partial recovery of an even Δj_1 propensity for *ortho*-D_2 collisions. Nevertheless, it appears that CN is sufficiently harmonic whose dependence on v_1 for pure rotational transitions is small.

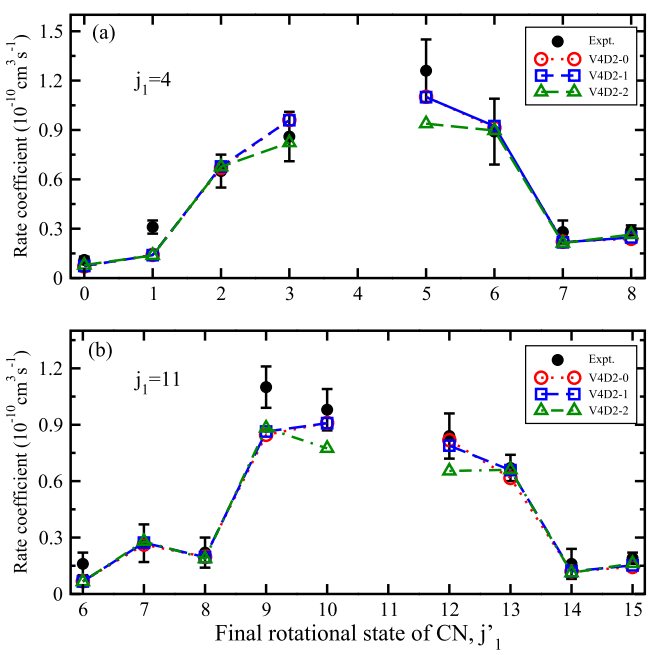

FIG. 9. Inelastic rotational rate coefficients for CN at T = 295 K for a statistical population of D_2 ($v_2 = 0, j_2 = 0, 1$), i.e., normal-D_2. (a) $j_1 = 4$, (b) $j_1 = 11$. Experiment[11] $v_1 = 2$ (solid circles) and current 4D theory $v_1 = 0$ (open circles), $v_1 = 1$ (open squares), and $v_1 = 2$ (open triangles).

Returning to the experiment, they were state-to-state measurements performed by laser probing the CN level populations and then using a master equation analysis to extract rate coefficients. For $v_1 > 0$, the level populations may also be quenched by reactive scattering to H + HCN and vibrational de-excitation, which are not considered in the experimental modeling. Vibrational quenching is typically many orders of magnitude smaller than rotational quenching but may become competitive for a quasi-resonant transition as found for CO–H_2[35] (e.g., the $1002 \rightarrow 0006 + 83\ \mathrm{cm}^{-1}$ transition, in CMS notation). For CN–H_2, the quasi-resonant transitions $1002 \rightarrow 0006 - 18\ \mathrm{cm}^{-1}$ and $2002 \rightarrow 1006 - 45\ \mathrm{cm}^{-1}$ are potentially relevant to the Brunet *et al.*[11] measurements. Both processes are slightly endoergic and will be studied in future work.

B. Scattering calculations for vibrational quenching

Full-dimensional quantum CC calculations of rovibrational cross sections were carried out for initial CMSs ($100j_2$), for *para*-H_2 ($j_2 = 0$) and *ortho*-H_2 ($j_2 = 1$) with collision energies ranging from 1 to 1000 cm^{-1}. In Figs. 10 and 11 the state-to-state quenching cross section to final states ($0j_1'0j_2$), $j_1' = 0, 2, 4, \ldots, 24$ are shown for *para*- and *ortho*-H_2, respectively, where $j_2 = j_2'$. The cross sections have similar behavior and display resonances at low energies due to quasibound states of the collision complex. Small $|\Delta j_1| = |j_1' - j_1|$ transitions dominate the quenching with the cross sections generally decreasing with increasing j_1' with that for $j_1' = 0$ being the largest. This indicates that the cross section is dominated by the strength of the interaction terms $A_{\lambda_1,\lambda_2,\lambda_{12}}$ and not by the asymptotic channel energy gaps.

The total cross sections $\sigma^{\mathrm{T}}_{v_1 j_1 v_2 j_2 \rightarrow v_1' v_2' j_2'}(E)$ for CN vibrational quenching from $v_1 = 1 \rightarrow v_1' = 0$ are given in Fig. 12. Fig. 12(a) shows the total cross section from (1000) to CN ($v_1' = 0$) + *para*-H_2 ($j_2' = 0, 2$), while Fig. 12(b) displays the total cross section from (1001) to CN ($v_1' = 0$) + *ortho*-H_2 ($j_2' = 1, 3$). The total vibrational quenching cross section display orbiting resonances between collision energies of 1.0 and 100 cm^{-1}. However, the magnitude of the resonances are suppressed for H_2 elastic processes, $j_2 = j_2'$. For both the *para*- and

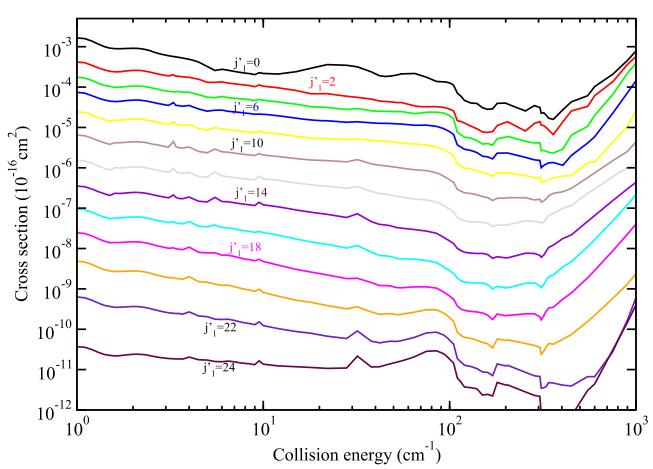

FIG. 10. State-to-state cross sections for the vibrational quenching of CN from ($v_1 = 1, j_1 = 0$) to ($v_1' = 0, j_1'$), $j_1' = 0, 2, 4, \ldots, 24$, due to *para*-$H_2$ ($v_2 = 0, j_2 = 0$) collisions, or in CMS notation (1000) → ($0j_1'00$), $j_2 = j'_2 = 0$.

RIGHTSLINK

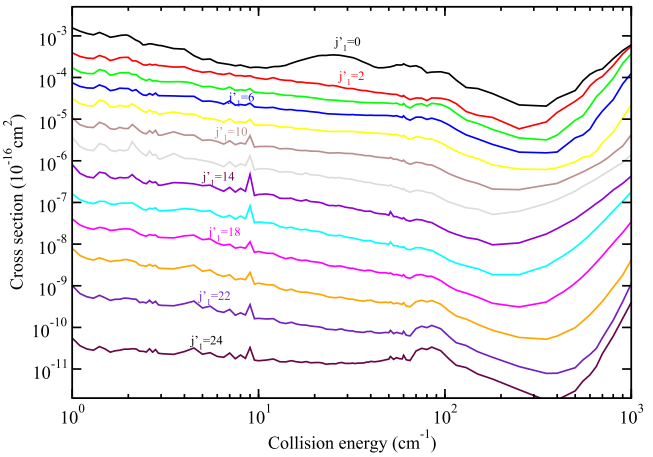

FIG. 11. State-to-state cross sections for the vibrational quenching of CN from ($v_1 = 1, j_1 = 0$) to ($v_1' = 0, j_1'$), $j_1' = 0, 2, 4, \ldots, 24$, by *ortho*-$H_2$ ($v_2 = 0$, $j_2 = 1$), or in CMS notation $(1001) \rightarrow (0j_1'01)$, $j_2 = j'_2 = 1$.

ortho-H_2 cases, the total vibrational quenching cross sections for elastic H_2 processes are nearly an order of magnitude larger than that for collisions involving inelastic H_2 transitions.

Total rate coefficients for the vibrational quenching of CN from (1000) to CN ($v_1' = 0$) + *para*-H_2 ($j_2' = 0$ and 2) and from (1001) to CN ($v_1' = 0$) + *ortho*-H_2 ($j_2' = 1$ and 3) are displayed in Fig. 13 for temperatures ranging from 5 to 300 K. The trends are similar to that given for the cross sections in Fig. 12. The total vibrational quenching rate coefficients of CN for $\Delta j_2 = 0$ are nearly an order of magnitude larger than the results for $\Delta j_2 = 2$. For the quenching due to *para*-H_2 collisions, as shown in Fig. 13(a), between 5 and ~100 K, the rate coefficients generally decrease weakly with increasing temperature, while weak oscillatory temperature dependences are exhibited due to the presence of resonances. For temperatures above

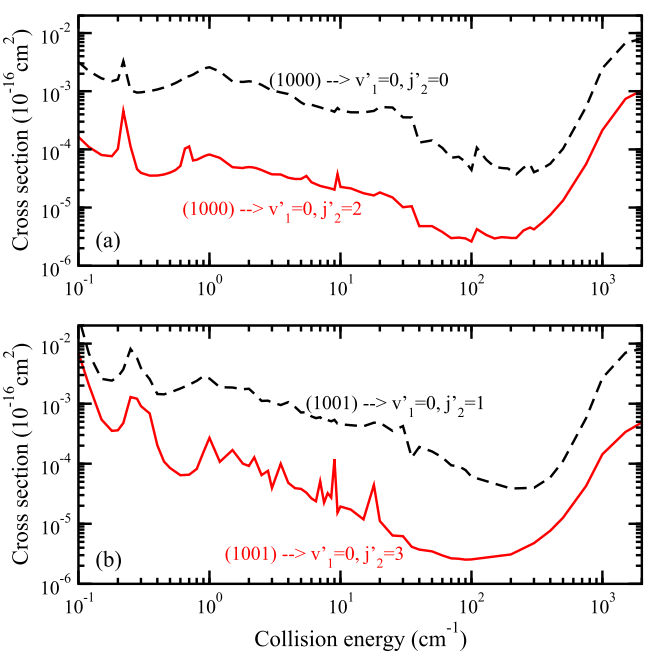

FIG. 12. Total cross sections for the vibrational quenching of CN (a) from (1000) to CN ($v_1' = 0$) + *para*-H_2 ($j_2' = 0$ and 2). (b) From (1001) to CN ($v_1' = 0$) + *ortho*-H_2 ($j_2' = 1$ and 3).

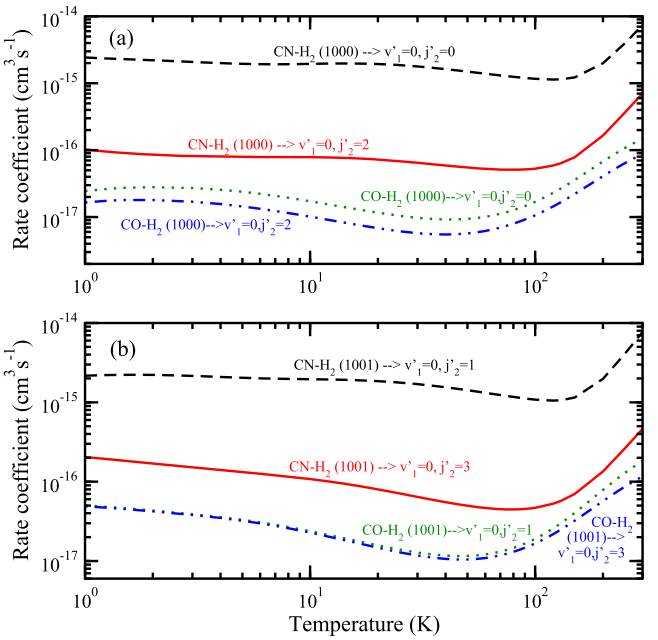

FIG. 13. Total rate coefficients for the vibrational quenching of CN compared to the same transitions for CO from Ref. 35. (a) From (1000) to $v_1' = 0$ + *para*-H_2 ($v_2 = 0, j_2' = 0, 2$). (b) From (1001) to $v_1' = 0$ + *ortho*-H_2 ($v_2 = 0$, $j_2' = 1, 3$).

~100 K, the rate coefficients increase with increasing temperature. The trends for *ortho*-H_2 are very similar to those noted for *para*-H_2 collisions. CO–H_2 rate coefficients[35] for the same transitions are typically factors of ~5-10 smaller, as shown in Fig. 13. The smaller CO–H_2 rate coefficients are likely related to the fact that the CN–H_2 potential is more anisotropic, e.g., with global and local minima deeper by 38.69 and 11.12 cm^{-1}, respectively.

V. DISCUSSION

As highlighted in the Introduction, in astrophysical environments with intense UV fields, the radiation can drive the chemistry and internal level populations out of equilibrium. In such situations, a photodissociation region (PDR) resides at the interface of the hot H II region and the cold molecular region. Sternberg and Dalgarno[40] investigated the production of gas-phase atomic and molecular species in dense molecular clouds and identified molecular diagnostics of photon-dominated chemistry. It was illustrated that CN was formed by photodissociation of HCN, HCN + $\nu \rightarrow$ CN + H, and by the reactions NO + C $\rightarrow$ CN + O and C + N $\rightarrow$ CN + ν. Minor production of CN can also be obtained from dissociative recombination $H_2CN^+ + e \rightarrow CN + H_2$. The CN abundance strongly depends on the UV radiation and increases in PDRs as the HCN photodissociation rate increases. Hence, CN emission lines may serve as useful diagnostics of PDRs.

Rodriguez-Franco and Martin-Pintado[9] reported the observations of the CN 1-0 and 2-1 rotational emission towards the Orion A molecular complex and showed that the ionized gas of the H II region dominated the morphology of the CN emission. Aalto *et al.*[10] detected CN 1-0 and 2-1 line emission in IR luminous galaxies and found that CN emission required

RIGHTSLINK

high density, $n > 10^4$ cm^{-3}. Therefore CN is expected to be a good tracer of high density regions and cold dense molecular clouds. This was also confirmed by Hakobian and Crutcher[41] in their multi-species study of structure and composition of molecular clouds through the CN Zeeman transitions. Finally, Podio *et al.*[42] argue that high j_1 lines, particularly the 5-4, are unique tracers of embedded disks of young stellar objects, such as T Tau N.

We are, however, unaware of any CN vibrational transition observations though it is predicted to be abundant in models of protoplanetary disks[43] and in the outflows of giant C- and O-rich evolved stars.[44,45] It is anticipated that vibrational emission lines can probe the hot inner wind regions of the outflows and therefore provide information on the stellar mass-loss rates.[44] With the upcoming launch of NASA's *James Webb Space Telescope*, the CN vibrational bands will become observable allowing astronomers to see deep into warm regions of these objects, particularly where the vibrational lines can be pumped by intense ultraviolet radiation. The collisional data computed here will be critical for models of such near infrared observations.

VI. CONCLUSION

Accurate collisional rate coefficients for CN due to H_2, needed for astrophysical modeling, are currently lacking for vibrationally excited CN. Quantum scattering calculations are the primary source of such rate coefficients, but accurate values that explicitly consider all six internal degrees of freedom of the CN–H_2 complex have not been reported due to the difficulty of the computations. We performed the first full-dimensional quantum dynamics calculations for inelastic rovibrational transitions of CN in collisions with H_2 using a high-level 6D PES. The PES was fitted with an invariant polynomial approach with an RMS error of less than 3.8 cm^{-1}. Cross sections and rate coefficients for rotational (de)excitation of CN due to H_2 and D_2 collisions were studied using the new 6D PES for excited initial rotational levels of CN (j_1 = 4 and 11). Good agreement with the results of previous theoretical and experimental studies confirms the accuracy of the current PES fit and scattering calculations. We have carried out the first calculations of rovibrational quenching of CN ($v_1 = 1, j_1 = 0$) in collisions with H_2 ($v_2 = 0, j_2 = 0, 1, 2$) on the new 6D PES. To aid in astrophysical modeling, computations are in progress for a more highly excited vibrational level of $v_1 = 2$ of CN.

SUPPLEMENTARY MATERIAL

See supplementary material[46] for a Fortran subroutine to generate V6ES PES.

ACKNOWLEDGMENTS

Work at UGA and Emory was supported by NASA Grant No. NNX12AF42G from the Astronomy and Physics Research and Analysis Program, at UNLV by NSF Grant No. PHY-1505557, and at Penn State by NSF Grant No. PHY-1503615. This study was supported in part by resources and technical expertise from the UGA Georgia Advanced Computing Resource Center (GACRC), a partnership between the UGA Office of the Vice President for Research and Office of the Vice President for Information Technology. We thank Shan-Ho Tsai (GACRC) and Jeff Deroshia (UGA Department of Physics and Astronomy) for computational assistance. We also thank Dr. Yulia Kalugina for providing their potential subroutine and cross-sectional data.

[1] E. F. van Dishoeck and J. H. Black, Astrophys. J. **340**, 273 (1989).
[2] K. Slyk, A. V. Bondar, G. A. Galazutdinov, and J. Krelowski, Mon. Not. R. Astron. Soc. **390**, 1733 (2008).
[3] A. McKellar, Publ. Astron. Soc. Pac. **52**, 187 (1940).
[4] A. Wootten, S. M. Lichten, R. Sahai, and P. G. Wannier, Astrophys. J. **257**, 151 (1982).
[5] A. M. Ritchey, S. R. Federman, and D. L. Lambert, Astrophys. J. **728**, 36 (2013).
[6] S. Guilloteau *et al.*, Astron. Astrophys. **549**, A92 (2013).
[7] P. Hily-Blant *et al.*, Astron. Astrophys. **557**, A65 (2013).
[8] B. Mookerjea *et al.*, Astron. Astrophys. **566**, A61 (2014).
[9] A. Rodriguez-Franco, A. Martin-Pintado, and A. Fuente, Astron. Astrophys. **329**, 1097 (1998).
[10] S. Aalto, A. G. Polatidis, S. Huttemeister, and S. J. Curran, Astron. Astrophys. **381**, 783 (2002).
[11] S. M. K. Brunet, J. Guo, T. Carrington, S. V. Filseth, and C. M. Sadowski, J. Chem. Phys. **116**, 3617 (2002).
[12] A. L. Kaledin, M. C. Heaven, and J. M. Bowman, J. Chem. Phys. **110**, 10380 (1999).
[13] A. L. Kaledin and M. C. Heaven, Chem. Phys. Lett. **347**, 199 (2001).
[14] Y. Kalugina, F. Lique, and J. Klos, Mon. Not. R. Astron. Soc. **422**, 812 (2012).
[15] Y. Kalugina, J. Klos, and F. Lique, J. Chem. Phys. **139**, 074301 (2013).
[16] X. H. Wang and J. M. Bowman, J. Chem. Theory Comput. **9**, 901 (2013).
[17] Y. Kalugina and F. Lique, Mon. Not. R. Astron. Soc. **446**, L21 (2015).
[18] D. R. Flower and F. Lique, Mon. Not. R. Astron. Soc. **446**, 1750 (2015).
[19] B. A. O'Donnell, A. Bridget, and J. M. Beames, J. Chem. Phys. **136**, 234304 (2012).
[20] T. B. Adler, G. Knizia, and H.-J. Werner, J. Chem. Phys. **127**, 221106 (2007).
[21] H.-J. Werner, T. B. Adler, and F. R. Manby, J. Chem. Phys. **126**, 164102 (2007).
[22] D. E. Woon and T. H. Dunning, J. Chem. Phys. **100**, 2975 (1994).
[23] H.-J. Werner, P. J. Knowles, G. Knizia, F. R. Manby, M. Schütz, P. Celani, T. Korona, R. Lindh, A. Mitrushenkov, G. Rauhut, K. R. Shamasundar, T. B. Adler, R. D. Amos, A. Bernhardsson, A. Berning, D. L. Cooper, M. J. O. Deegan, A. J. Dobbyn, F. Eckert, E. Goll, C. Hampel, A. Hesselmann, G. Hetzer, T. Hrenar, G. Jansen, C. Köppl, Y. Liu, A. W. Lloyd, R. A. Mata, A. J. May, S. J. McNicholas, W. Meyer, M. E. Mura, A. Nickla, D. P. O'Neill, P. Palmieri, D. Peng, K. Pflüger, R. Pitzer, M. Reiher, T. Shiozaki, H. Stoll, A. J. Stone, R. Tarroni, T. Thorsteinsson, and M. Wang, MOLPRO, version 2010.1, a package of *ab initio* programs, 2010, see http://www.molpro.net.
[24] F. Bernardi and S. F. Boys, Mol. Phys. **19**, 553 (1970).
[25] D. P. Tew and W. Klopper, J. Chem. Phys. **125**, 094302 (2006); D. Feller, K. A. Peterson, and J. G. Hill, *ibid.* **133**, 184102 (2010).
[26] J. M. Bowman, G. Czakó, and B. N. Fu, Phys. Chem. Chem. Phys. **13**, 8094 (2011).
[27] B. J. Braams and J. M. Bowman, Int. Rev. Phys. Chem. **28**, 577 (2009).
[28] K. Takayanagi, Adv. At. Mol. Phys. **1**, 149 (1965).
[29] S. Green, J. Chem. Phys. **62**, 2271 (1975).
[30] M. H. Alexander and A. E. DePristo, J. Chem. Phys. **66**, 2166 (1977).
[31] G. Zarur and H. Rabitz, J. Chem. Phys. **60**, 2057 (1974).
[32] A. M. Arthurs and A. Dalgarno, Proc. R. Soc. A **256**, 540 (1960).
[33] G. Quéméner and N. Balakrishnan, J. Chem. Phys. **134**, 214303 (2011).
[34] S. Fonseca dos Santos, N. Balakrishnan, S. Lepp, G. Quéméner, R. C. Forrey, R. J. Hinde, and P. C. Stancil, J. Chem. Phys. **134**, 214303 (2011).
[35] B. H. Yang, P. Zhang, X. Wang, P. C. Stancil, J. M. Bowman, N. Balakrishnan, and R. C. Forrey, Nat. Commun. **6**, 6629 (2015).
[36] R. V. Krems, *TwoBC—Quantum Scattering Program* (University of British Columbia, Vancouver, Canada, 2006).
[37] B. R. Johnson, J. Comput. Phys. **13**, 445 (1973).
[38] D. E. Manolopoulos, J. Chem. Phys. **85**, 6425 (1986).

RIGHTSLINK

[39]J. M. Hutson and S. Green, molscat computer code version 14, distributed by Collaborative Computational Project No. 6 of the United Kingdom Engineering and Physical Sciences Research Council, Swindon, 1994.
[40]A. Sternberg and A. Dalgarno, Astrophys. J., Suppl. Ser. **99**, 565 (1995).
[41]N. S. Hakobian and R. M. Crutcher, Astrophys. J. **733**, 6 (2011).
[42]L. Podio, I. Kamp, C. Codella, B. Nisini, G. Aresu, S. Brittain, S. Cabrit, C. Dougados, C. Grady, R. Meijerink, G. Sandell, M. Spaans, W.-F. Thi, G. J. White, and P. Woitke, Astrophys. J. **783**, L26 (2014).
[43]C. Walsh, T. J. Millar, and H. Nomura, Astrophys. J. **722**, 1607 (2010).
[44]L. Decin, E. De Beck, S. Brünken, H. S. P. Müller, K. M. Menten, H. Kim, K. Willacy, A. de Koter, and F. Wyrowski, Astron. Astrophys. **516**, A69 (2010).
[45]X. Li, T. J. Millar, C. Walsh, A. N. Heays, and E. F. van Dishoeck, Astron. Astrophys. **568**, A111 (2014).
[46]potV6ES.f is a Fortran subroutine to generate V6ES PES. Distances are in bohr, angles are in radian, and potential energy is in hartree. FitCoef.dat is the file for fitted coefficients of V6ES.

RIGHTSLINK